Pnictogen-Bonding Catalysis Compared with Ion Transport in Lipid Bilayer Membranes: Entering the Goldilocks Inverted Region

Zhang, Qing-Xia; Renno, Giacomo; Nué-Martinez, J. Jonathan; Besnard, Céline; Gomila, Rosa M.; Frontera, Antonio; Sakai, Naomi; Matile, Stefan

How to cite

ZHANG, Qing-Xia et al. Pnictogen-Bonding Catalysis Compared with Ion Transport in Lipid Bilayer Membranes: Entering the Goldilocks Inverted Region. In: CCS Chemistry, 2025, vol. 7, n° 1, p. 91–104. doi: 10.31635/ccschem.024.202404847

This publication URL: https://archive-ouverte.unige.ch/unige:184332

Publication DOI: 10.31635/ccschem.024.202404847

CCS Chemistry

RESEARCH ARTICLE

Received: Aug. 5, 2024 | Accepted: Aug. 28, 2024 | Published: Sept. 26, 2024

Pnictogen-Bonding Catalysis Compared with Ion Transport in Lipid Bilayer Membranes: Entering the Goldilocks Inverted Region

Qing-Xia Zhang[1], Giacomo Renno[1], J. Jonathan Nué-Martinez[1], Celine Besnard[1], Rosa M. Gomila[2], Antonio Frontera[2], Naomi Sakai[1] & Stefan Matile[1]*

[1]*School of Chemistry and Biochemistry, University of Geneva, CH-1211 Geneva,* [2]*Departament de Química, Universitat de les Illes Balears, SP-07122 Palma de Mallorca*

**Corresponding author: stefan.matile@unige.ch*

Cite this: *CCS Chem.* **2025**, 7, 91–104
DOI: 10.31635/ccschem.024.202404847

Antimony-centered pnictogen bonds at the stibine level have provided access to good catalysis in solution and outstanding ion transport and catalysis in lipid bilayer membranes. Strengthened pnictogen bonds on the stiborane level have increased catalytic activity in solution to an extent attractive for use in practice. Thus, the debate was whether or not transport and catalysis in lipid bilayer membranes would equally increase from σ-acidic stibines to σ-acidic stiboranes. The response, we report, is no. Experimental support for this conclusion covers a new set of σ-acidic catecholatostiborane catalysts with bioinspired catecholates, supramolecular structural X-ray and computational data, transfer hydrogenation catalysis in water, micelles and membranes, and, of course, ion transport across lipid bilayers. Decreasing ion transport with increasing ion binding defined the inverted region in the Goldilocks principle. Our results placed σ-acidic stibines with weaker pnictogen bonds in the well-explored Goldilocks normal region. σ-acidic stiboranes, however, with their strong pnictogen bonds, provided unprecedented access to the Goldilocks inverted region and emerged as unique tools to generalize the Goldilocks principle from transport to catalysis and from membranes to micelles. The reported methods and results should be of general interest in the design and rationalization of supramolecular function in biphasic systems.

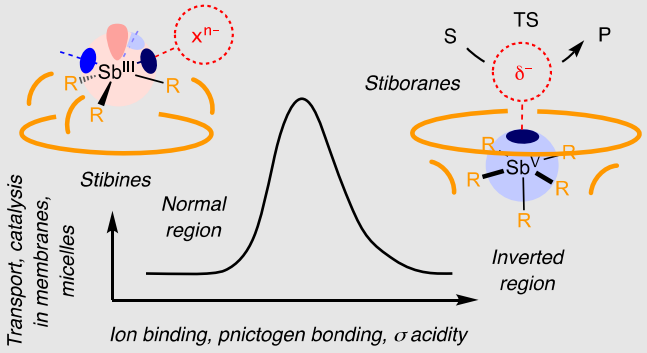

Keywords: **pnictogen bonds, catalysis, ion transport, stibines, stiboranes, σ acidity**

Introduction

Pnictogen bonds describe the noncovalent interaction of highly localized electron-deficient areas on pnictogens, so-called σ-holes, with electron-rich motifs, usually lone pairs (Figure 1a–d).[1–6] σ-Holes relate to antibonding σ* orbitals, with orbital contributions accounting for pnictogen and the analogous chalcogen and halogen bonds to extend linearly from the respective covalent bond with high directionality.[1–10] σ-Hole interactions increase with

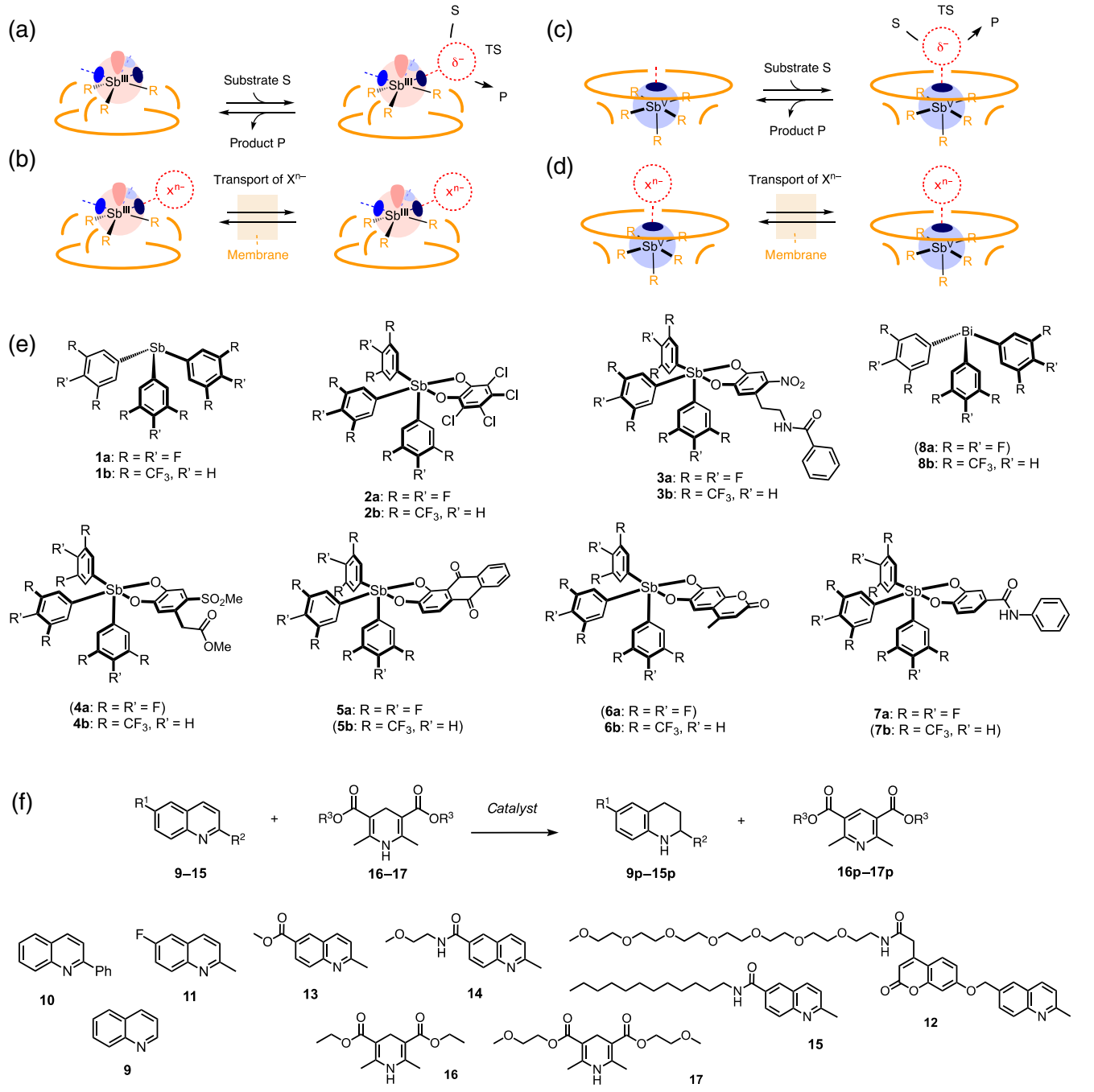

Figure 1 | *(a, c) Catalysis and (b, d) ion transport with (a, b) σ-acidic stibines and (c, d) stiboranes, and structure of (e) pnictogens **1–8** and (f) substrates **9-17** used in this study. (a, b) Stibines offer three σ-holes (blue) on their more convex surface (gold), extending linearly from the three covalent bonds (black) to (a) stabilize electron-rich centers of transition states (δ⁻, TS) for catalysis and (b) bind anions (X^{n-}) for transport. (c, d) Stiboranes offer one deep σ-hole on their more convex surface, extending linearly from the axial Sb-C bond, for (c) TS stabilization and (d) X^{n-} transport. Compounds with numbers in parentheses are only virtual.*

polarizability. In 2018, a comprehensive screen of the relevant piece of the periodic table evinced pnictogen bonds with Sb(III) centers as the most promising σ-hole interaction for catalysis.[11] In the same year, the addition of catecholates to Sb(III) stibines was shown to afford Sb(V) stiboranes with increased catalytic activity.[12] Electron-deficient stibines offer three σ-holes exposed on an overall more convex surface, surrounding the central lone pair in the linear extension of the three covalent bonds (Figure 1a,b). Catecholate addition to these

DOI: 10.31635/ccschem.024.202404847
Citation: *CCS Chem.* **2025**, 7, 91–104
Link to VoR: https://doi.org/10.31635/ccschem.024.202404847

stibines converts the three σ-holes into one deep σ-hole on electron-deficient stibines, embedded within an overall more concave surface (Figure 1c,d).

Since these initial studies, pnictogen-bonding and the related chalcogen- and halogen-bonding catalysis[1-3,8,11-25] have been tentatively defined as the noncovalent counterpart of classical Lewis acid catalysis, just like hydrogen-bonding catalysis is the supramolecular counterpart of Brønsted acid catalysis.[26] One of the distinguishing characteristics of pnictogen-bonding catalysts with permanent substituents compared with classical Lewis acids like $SbCl_3$ with exchangeable ligands is their usually good stability in aqueous systems,[27,28] including artificial enzymes.[29] Incompatible with classical Lewis acids like $SbCl_3$, a systematic screen revealed that σ-acidic stibines are also outstanding ion transporters (Figure 1b) and that their catalytic activity in lipid bilayer membranes increases strongly in comparison with organic solvents.[30] With σ-acidic stiboranes being more active catalysts than σ-acidic stibines in organic solvents (Figure 1c vs a), the question was whether or not stiboranes would also outperform stibines as anion transporters (Figure 1d vs b) and catalysts in lipid bilayer membranes. If so, we envisaged that this would result in spectacular activities considering the already high activity identified for stibines.[30,31] The objective of this study was to address this question with a series of pnictogen-bonding systems **1**–**8** (Figure 1e) and transfer hydrogenation[18,20,28,29] with substrates **9**–**17** as a robust benchmark reaction (Figure 1f).

Experimental Methods

Synthesis

Representative procedure for catalyst **6b**: To a suspension of **1b** (0.38 g, 0.50 mmol) in tetrahydrofuran (THF, 10 mL), the corresponding coumarin (0.10 g, 0.50 mmol) and ^{t}BuOOH (110 μL of 5.0 M solution in nonane, 0.55 mmol) were added at 0 °C. After 2 h, the reaction was warmed to room temperature and stirred overnight. Then transparent solution formed was evaporated to dryness. The crude product was recrystallized with diethyl ether/pentane, acetone/pentane, CH_2Cl_2/pentane, $CHCl_3$/pentane, and toluene/pentane, finally affording the pure compound **6b** (81 mg, 17%) as a yellow solid. Mp: 171–172 °C; infrared (IR; neat): 1634 (s, C=O), 1539 (s), 1491 (s), 1556 (w), 1175 (s, CO), 1089 (s), 1032 (s), 859 (s), 681 (s); ^{1}H nuclear magnetic resonance (NMR) (500 MHz, acetone-d_6): 8.49 (s, 6H), 8.26 (s, 3H), 7.18 (s, 1H), 6.82 (s, 1H), 6.02 (s, 1H), 2.37 (s, 3H); ^{13}C NMR (126 MHz, acetone-d_6): 162.1 (CO), 154.5 (C), 152.3 (C), 149.3 (C), 145.2 (3C), 145.1 (C), 135.7 (6CH, q, $^3J_{C\text{-}F}$ = 3.8 Hz), 132.5 (6C, q, $^2J_{C\text{-}F}$ = 33.2 Hz), 125.8 (3CH, sept, $^3J_{C\text{-}F}$ = 3.8 Hz), 124.2 (6C, q, $^1J_{C\text{-}F}$ = 272.5 Hz), 112.7 (C), 111.5 (CH), 107.5 (CH), 102.1 (CH), 19.0 (CH_3); ^{19}F NMR (282 MHz, acetone-d_6): −63.45.

Other catalysts and substrates were prepared correspondingly, following reported procedures if possible[12,28,29,32-34] (Supporting Information Figures S1, S2, S33–S51 and Schemes S1–S7).

Structural Characterization

The single crystals of **2a**, **3a**, and **3b** were obtained by dissolving each in Et_2O/hexane and allowing their Et_2O/hexane solutions to evaporate at room temperature. The X-ray intensity data of the crystals were acquired using a Rigaku XtaLAB Synergy, Dualflex, HyPix-Arc 150° diffractometer using Cu Kα radiation (λ = 1.54184 Å).

In computational modeling, the geometries of the compounds and complexes in this study were fully optimized without any constraints at the RI-BP86-D4/def2-TZVP level of theory.[35-37] Calculations were performed in the gas phase using the TURBOMOLE version 7.7 program.[38] The minimum nature of the compounds was confirmed by frequency calculations. The molecular electrostatic potential (MEP) surface calculations were plotted using the Gaussian-16 program[39] at the same level of theory, with MEP surfaces plotted using the 0.001 a.u. isosurface. Polarizability calculations were performed at the same level using TURBOMOLE version 7.7.[38] The quadrupole moments were calculated using the Multiwfn program[39-41] with wavefunctions generated by TURBOMOLE version 7.7[38] at the same level of theory.

Preparation of EYPC-LUVs

Large unilamellar vesicles (LUVs) were prepared from egg yolk phosphatidylcholine (EYPC) following reported procedures.[30,31] Briefly, EYPC (25.0 mg) was dissolved in $CHCl_3$ (1 mL). The solution was evaporated on a rotary evaporator (40 °C), and then a lipid film was dried in vacuo for 1 day. After hydration (>30 min) with 1.0 mL buffer [100 mM NaCl or 67 mM Na_2SO_4, 10 mM HEPES, 1.0 or 1.0 mM HPTS (a fluorescent probe), pH 7.0 at 40 °C (HEPES: (4-(2-hydroxyethyl)-1-piperazineethanesulfonic acid); HPTS: 8-Hydroxypyrene-1,3,6-trisulfonic acid trisodium salt), the resulting suspension was subjected to >10 freeze-thaw cycles (liquid N_2, 40 °C water bath) and >10 times extruded through a polycarbonate membrane (pore size 100 nm). In the presence of HPTS in NaCl solution, extravesicular components were removed by size exclusion chromatography (Sephadex G-50, Cytiva, Marlborough, USA) with 10 mM HEPES, 100 mM NaCl, pH 7.0 buffer. Final conditions: ≈6 mL of 5 mM EYPC, inside and outside 10 mM HEPES, 100 mM NaCl, or 67 mM Na_2SO_4, pH 7.0. The EYPC-LUVs - were used within the week of preparation.

Ion transport

Following previously reported procedures,[30] a suspension of EYPC-LUVs⊃HPTS (20 μL) was added to a gently

DOI: 10.31635/ccschem.024.202404847
Citation: *CCS Chem.* **2025**, 7, 91–104
Link to VoR: https://doi.org/10.31635/ccschem.024.202404847

stirred, thermostatically controlled buffer (1920 μL, 25 °C, 10 mM HEPES, 100 mM NaCl, pH 7.0) in an optical glass cuvette, The fluorescence intensity (λ_{em} = 510 nm) was monitored as a function of time upon excitation at two wavelengths simultaneously ($I_{t,454}$: λ_{ex} = 454 nm and $I_{t,404}$: λ_{ex} = 404 nm) during the addition of compound [20 μL, dimethyl sulfoxide (DMSO) solution] at t = 1 min, base (20 μL, 0.5 M NaOH) at t = 2 min and gramicidin D (20 μL, 1 μM in DMSO) at t = 6 min 45 s. Ratiometric analysis of the kinetic traces ($R_t = I_{t,454}/I_{t,404}$) was performed by normalization to $R_0 = R_t$ at t = 2 min, before addition of base, and $R_\infty = R_t$ at t = 7 min 30 s, after addition of gramicidin D. I_{rel} at 6 min 38 s before addition of gramicidin D was defined as transmembrane activity, Y_c. Hill analysis of the concentration dependence of Y_c gave the effective concentration EC_{50} and the Hill coefficient n.

Catalysis in vesicles

In a 0.5 mL Eppendorf tube, quinoline **14** and **15** (1.6 μL of a 50 mM stock solution in DMSO, final concentration 0.31 mM), the catalyst **2b** (1.6 μL of a 15 mM stock solution in DMSO, final concentration 0.094 mM) the internal standard 7-(diethylamino)-4-methyl-2*H*-chromen-2-one (for **14**, 1.6 μL of a 5.0 mM stock solution in DMSO, final concentration 0.031 mM; For **15**, 1.6 μL of a 2.5 mM stock solution in DMSO, final concentration 0.016 mM) and DMSO (1.3 μL) were added. Subsequently, 240 μL HEPES buffer (pH = 7.0) and 2.5 μL EYPC-LUVs were sequentially added to the mixture, and finally, the Hantzsch ester **16** (1.6 μL of a 150 mM stock solution in DMSO, final concentration 0.94 mM). The reaction was then shaken (800 rpm) at 40 °C. Periodically, aliquots (4.8 μL) of the reaction mixture were diluted in CH_3CN (2000 μL, final concentration [**14** + **14p**], [**15** + **15p**] = 0.74 μM), and their fluorescence spectra were recorded (λ_{ex} = 320 nm). Calibration curves were applied to calculate substrate conversion from the measured intensity ratios.

Other catalysts and substrates were measured correspondingly, see Supporting Information.

Catalysis in micelles

In a 0.5 mL Eppendorf tube, 25 μL (27 mg) Triton X-100 was added. Then the following was added to the mixture: quinoline **15** (5.0 μL of a 50 mM stock solution in DMSO, final concentration 1.0 mM), catalysts **1**–**4** (5.0 μL of a 15 mM stock solution in DMSO, final concentration 0.30 mM), the internal standard [7-(diethylamino)-4-methyl-2*H*-chromen-2-one, 5.0 μL of a 2.5 mM stock solution in DMSO, final concentration 0.050 mM] and 5.0 μL DMSO. Subsequently, 200 μL HEPES buffer (pH = 7.0) and the Hantzsch ester **16** (5.0 μL of a 150 mM stock solution in DMSO, final concentration 3.0 mM) were sequentially added into the mixture. The reaction was then shaken (800 rpm) at 30 °C. Periodically, aliquots (3.0 μL) of the reaction mixture were taken to determine substrate conversion with time.

Catalysis in solution

Following previously reported procedures,[42] the catalyst and substrates were weighted into a screw cap vial and suspended in excess dry $CDCl_3$ or dry CD_3CN. The mixture was degassed by argon bubbling until the desired final solvent volume was reached, comprising substrate **10** (128 mM), Hantzsch ester **16** (281 mM), the desired catalyst (30 mol %, 38 mM) and mesitylene (43 mM, internal standard). The vial was tightly sealed and stirred at 40 °C. ^{1}H NMR spectra of aliquots of the reaction mixture (20 μL) diluted in $CDCl_3$ (0.5 mL) were recorded at varying time intervals (Supporting Information Figures S9–S12).

Results and Discussion

Pnictogen-bonding systems

Stibines and stiboranes **1**–**8** were selected for this study for the following reasons. Originally, σ-acidic stibine catalysts were made with three electron-withdrawing pentafluorophenyl substituents to deepen the σ-holes on the Sb(III) center and to lower the lowest unoccupied molecular orbital (LUMO).[11] The fluorines at the *ortho* position were replaced by hydrogens in stibine **1a** despite decreasing σ acidity to avoid inactivation by intramolecular pnictogen bonds.[32,43] This change resulted in high transport[30,31] and catalytic activity[30] in lipid bilayer membranes. In a recent detailed study, Beer and coworkers[44] showed that the two CF_3 substituents at the *meta* position gave the best anion binding in the antimony series with **1b** and in the bismuth series with **8b**.

On the Sb(V) level, catecholato-stiborane **2b**, the oxidation product of **1b** with o-chloranil, was already reported as a good catalyst in the original paper by Gabbaï and coworkers,[12] and catalysis with **2a** and other derivatives has also been reported.[26,29,32,43] To explore the structural landscape on the catecholate side, we considered the bioinspired motifs that have been mapped out to access stable boronate esters for the discovery of the third orthogonal covalent bond.[33] Nitrodopamides, previously explored by Gademann and coworkers as biomimetic adhesives,[45] have emerged as the best performing catechols in that study.[33] The corresponding σ-acidic stiboranes like **3** were easily accessible and have already been identified as the best cofactor in pnictogen-enzymes.[29] In the screen for stable boronate esters, catechols with sulfonate acceptors as in stiborane **4** were almost as good as nitrodopamides in stiborane **3**.[33] The colorful alizarin red in stiborane **5** and coumarin as in stiborane **6** were added out of curiosity. The

DOI: 10.31635/ccschem.024.202404847
Citation: *CCS Chem.* **2025**, 7, 91–104
Link to VoR: https://doi.org/10.31635/ccschem.024.202404847

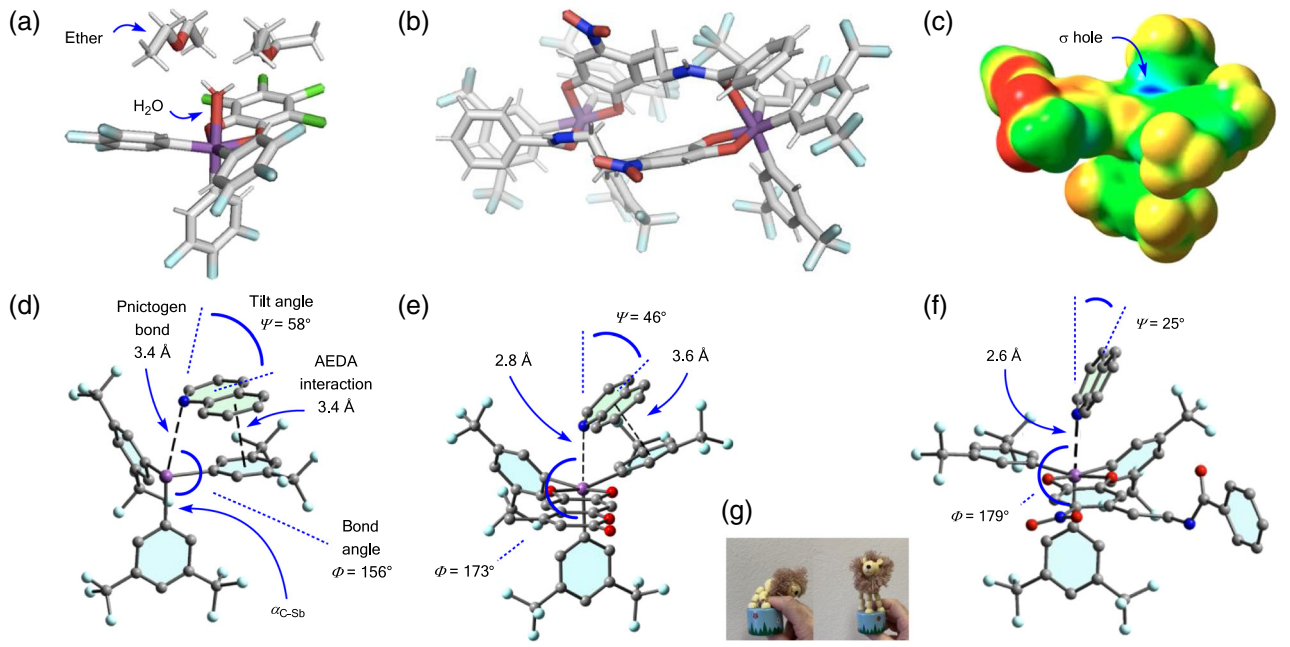

Figure 2 | *(a) X-ray structure of **2a** with pnictogen bond to H_2O (2.3 Å) and hydrogen bonds to two ethers (Sb-O catecholate: 2.1, 2.0). (b) X-ray structure of **3b** as pnictogen-bonded dimer (2.4 Å). (c–f) Computed structures, (c) BP86-D4/def2-TZVP level MEP surface of catalyst **4b**, blue positive (+52 kcal mol^{-1} max), red negative (–15 kcal mol^{-1} min), and structure of substrate **9** pnictogen-bonded to (d) catalyst **1b**, (e) **6b** and (f) **3b**. Computed structural data for all catalysts: Table 1. (g) Stand-up thumb push lion illustrating substrate motion in response to increasing σ acidity of pnictogen-bonding catalysts from **1b** to **6b** and **3b**.*

simple amide in stiborane **7** was of interest for the integration into more complex systems, including artificial enzymes.[29] The synthesis of all new pnictogen-bonding systems was achieved by adapting established procedures (Supporting Information Schemes S1–S5).

Structural studies

Over the years, several crystal structures of stibines and stiboranes have been reported.[12,32,46] Supra-structures with relevance beyond structural validation were obtained with crystals of stiborane **2a** grown in wet ether (Figure 2a and Supporting Information Figure S24 and Table S2). Namely, water was bound to the σ-hole of stiborane **2a**. Two hydrogen bonds to two ether molecules (1.9 Å) demonstrated that it is indeed water and not OH^- acting as an intermolecularly activated pnictogen-bond acceptor. The length of the Sb–O pnictogen bond to water was 2.3 Å. This was longer than the sum of covalent radii, 2.05 Å.[47] In the crystal structure of **2a**, the covalent Sb–O bonds to the catecholate had exactly this length.

Nitrodopamides **3a** and **3b** crystallized reproducibly as dimers with intermolecular pnictogen bonds to the amide oxygens (Figure 2b and Supporting Information Figures S25 and S26, Tables S3 and S4). The length of these O–Sb pnictogen bonds was 2.4 Å, that is, noncovalent, while the covalent O–Sb bonds with the catecholate were again around 2.05 Å.

The MEP surfaces of all pnictogen-bonding systems were computed on the BP86[S9]-D4/def2-TZVP level of theory (Figure 2c and Supporting Information Figures S27–S29). On these MEP surfaces, σ-holes appeared as deep blue dots, which were quantified with the respective surface potential maxima (Table 1). Although other contributions should not be ignored,[2] increasing depth of σ-holes roughly correlated with increasing "σ acidity," which translated into stronger pnictogen bonds.

The significant deepening of the σ-hole (V_{max}) from stibine **1a** to stiborane **2a** has already been reported (Table 1, entry 1 vs 3).[26] Further deepening on the Sb(V) level from 3,4,5-trifluorophenyls in stiborane **2a** to bis(trifluoromethyl)phenyls in stiborane **2b** by $\Delta V_{max} \approx 5$ kcal mol^{-1} was also known[28] (Table 1, entry 3 vs 4) and observed reliably throughout the series. Stiboranes **3**–**7** were naturally confirmed to be more σ-acidic than stibines **1**, **2**, and **8** (Table 1). Catecholate variations were less impactful. This was reasonable because they were not directly conjugated to the relevant σ* orbital. The deepest σ-hole V_{max} = +50.6 kcal mol^{-1} was found with the nitrodopamine catecholate in stiborane **3b** (Table 1, entry 6, Figure 2b,f).[29] Replacement of nitro acceptor in stiborane **3b** by a sulfone acceptor in stiborane **4b** caused a significant decrease of ΔV_{max} = –2.5 kcal mol^{-1}

DOI: 10.31635/ccschem.024.202404847
Citation: *CCS Chem.* **2025**, 7, 91–104
Link to VoR: https://doi.org/10.31635/ccschem.024.202404847

Table 1 | *Structural Characteristics*[a]

	C[b]	V_{max}[c]	α_{iso}[d]	$\alpha_{Sb\text{-}C}$[e]	*l* (Å)[f]	Φ (°)[g]	Ψ (°)[h]	π (Å)[i]
1	**1a**	+29.4	263	272	3.53	158	61	3.33
2	**1b**	+36.7	342	352	3.36	156	58	3.38
3	**2a**	+44.2	408	319	2.57	179	19	—[j]
4	**2b**	+49.3	488	392	2.50	177	25	—[j]
5	**3a**	+45.5	511	403	2.60	179	21	—[j]
6	**3b**	+50.6	591	475	2.59	179	25	—[j]
7	**4a**	+43.3	445	360	2.89	177	51	3.72[k]
8	**4b**	+48.1	525	422	2.79	175	46	3.75[k]
9	**5a**	+43.0	482	341	2.98	172	54	3.42[l]
10	**5b**	+47.1	562	412	2.84	175	54	3.72[k]
11	**6a**	+43.9	430	321	2.79	175	46	3.63[k]
12	**6b**	+48.5	510	394	2.75	173	46	3.56[k]
13	**7a**	+43.2	474	345	2.79	175	46	3.76[k]
14	**7b**	+48.0	554	413	2.75	173	46	3.58[k]
15	**8a**	+34.1	269	277	3.36	157	59	3.35[k]
16	**8b**	+40.4	349	458	3.27	158	64	3.51[k]

[a] From BP86[S9]-D4/def2-TZVP structures, Figure 2c–f and Supporting Information Figures S27–S31.
[b] Catalyst.
[c] Surface potential maximum (= σ-hole), in kcal mol^{-1}.
[d] Global polarizability, in a.u.
[e] Polarizability of axial Sb-C bond in Sb(V) compounds. For the Pn(III) compounds it is given along one of the Pn–C bonds, in a.u.
[f] Length of the pnictogen bond to substrate **9**.
[g] Angle of the pnictogen bond to **9**.
[h] Tilt angle of the quinoline plane from the pnictogen bond.
[i] Distance between the ring centroids of the substrate and the nearest aromatic ring in the catalyst, informing on secondary AEDA interactions.
[j] No AEDA interactions.
[k] Centroid of the N-ring of quinoline is used to measure the distance.
[l] AEDA interactions established with the quinone ring.

(Table 1, entry 6 vs 8). Similar σ acidity was achieved with coumarins in stiborane **6b** (entry 12) and amides in stiborane **7b** (entry 14), while alizarin red produced the weakest σ-holes in stiborane **5b** (entry 10), ΔV_{max} = –3.5 kcal mol^{-1} weaker than the best V_{max} = +50.6 kcal mol^{-1} with the nitrodopamide **3b** (Table 1, entry 6 vs 10).

While catecholate substitution in stiboranes had little influence on the depth of the σ-holes, it affected polarizability more significantly. From the chloranil original **2b** to the nitrodopamide **3b**, the σ-hole deepened by 3% to V_{max} = +50.6 kcal mol^{-1}, while global polarizability grew by 21% to a maximum of 591 a.u. (Table 1, entry 4 vs 6). The responsiveness of polarizability was unique to catecholate substituents. Changing the phenyl substituents from **2a** to **2b** caused a much larger 12% increase of the σ-hole, while the coinciding 20% increase in polarizability was less than with catecholate change from **2b** to **3b** (Table 1, entries 3, 4, 6).

Within the catecholate series, trends with σ-holes and global polarizability were not uniform. The relatively deep σ-hole V_{max} = +48.5 kcal mol^{-1} of coumarin **6b** coincided with weak α_{iso} = 510 a.u., the poorer V_{max} = +47.1 kcal mol^{-1} of alizarin red **5b** with second best α_{iso} = 562 a.u. (Table 1, entries 10, 12). Global polarizability α_{iso} and polarizability $\alpha_{Sb\text{-}C}$ along the axial bond with a σ* orbital at the σ-hole showed identical trends with overall minor exceptions.

Substrate-catalyst complexes were computed with the simplest possible quinoline **9** (Figure 1). The representative complexes with stiboranes **6b** and **3b** both featured a central pnictogen bond between the Sb(V) center and the quinoline nitrogen (Figure 2e,f). With **6b**, the length of 2.8 Å was indicative of a strong interaction that was clearly noncovalent, far beyond the sum of covalent radii at 2.10 Å (Figure 2e, Table 1, entry 12). The bond angle Φ = 173° was near the ideal Φ = 180° of σ-hole interactions. The quinoline plane was tilted by Ψ = 46° from the pnictogen bond, presumably to maximize aromatic electron donor–acceptor (AEDA) interactions with one phenyl substituent.[48,49] These AEDA interactions nicely illustrated the possibility of secondary interactions with the convex surface surrounding the σ-hole of Sb(V)

DOI: 10.31635/ccschem.024.202404847
Citation: *CCS Chem.* **2025**, 7, 91–104
Link to VoR: https://doi.org/10.31635/ccschem.024.202404847

Table 2 | *Rate Enhancements re_c in Organic Solvents*[a]

	C[b]	**10**[c]	**11**[d]	C[b]	**10**[c]	**11**[d]
1	**1a**	1	3	**1b**	13	50
2	**2a**	450	610	**2b**	150	490
3	**3a**	—	—	**3b**[e]	110	760
4	**4a**	—	—	**4b**	260	240
5	**5a**	220	60	**5b**	—	—
6	**6a**	—	—	**6b**	280	380
7	**7a**	230	340	**7b**	—	—
8	**8a**	—	—	**8b**	<1[f]	<1[f]
9	**2a**	9600	480	**2b**	—	—
10	**3a**	5880	540	**3b**	7700	610
11	**4a**	—	—	**4b**	6580	510

[a] $re_c = k_{cat}/k_{uncat}$ in $CDCl_3$ (entries 1–8) and CD_3CN (entries 9–11), from initial rates determined by ^1H NMR kinetics for 128 mM quinoline (**10**, **11**), 2.2 equiv hydride donor **16**, 30 mol % C and 33 mol % mesitylene (internal standard) at 40 °C. Experimental data: Supporting Information Figures S10–S12.
[b] Catalysts.
[c] re_c for **10**.
[d] re_c for **11** in $CDCl_3$.
[e] Poor solubility of catalyst, results might be underestimates.
[f] No conversion within 2 days.

catalysts (Figure 1c). Computed quadrupole moments Q_{zz} = –19.1 B confirmed quinoline substrates as π basic. Q_{zz} = +9.5 B and Q_{zz} = +10.9 B identified $RSbF_2$ mimics of F_3Ph **a** and $(CF_3)_2Ph$ **b** as slightly more π acidic than the hexafluorobenzene standard (Supporting Information Figure S32). Opposite signs of the quadrupole moments Q_{zz} in substrate and catalyst confirmed the possibility of AEDA interactions in their complex.

Deepening of the σ-hole made the quinoline substrate literally stand up, like a thumb push puppet (Figure 2g). The bond length was shortened to 2.6 Å for **3b**, the bond angles increased up to Φ = 179°—one degree from perfection (Figure 2f, Table 1, entry 6). The quinoline tilt decreased down to Ψ = 25° and AEDA interactions vanished. This coupled motion of the substrate in response to σ-hole deepening testified to a subtle balance between primary pnictogen bonding and secondary aromatic interactions with the concave surroundings of stiborane catalysts.

Weakening of the σ-hole from stiboranes to stibines made the quinoline substrate fully laid down (Figure 2d,g, Table 1, entry 2). The longer pnictogen bond (3.4 Å) expected from weaker σ acidity (+36.7 kcal mol^{-1}) allowed the pnictogen-bond angle in **1b** to decrease (Φ = 156°) and the substrate to tilt (Ψ = 58°) and interact with the π acids even on the convex surrounding, affording the best AEDA interactions found in the entire series (3.4 Å). During hydride addition, the secondary AEDA interactions should evolve into stronger anion-π interactions[50–52] that could support the primary pnictogen bonds to strengthen the hydride acceptor.

Catalysis in organic solvents

Transfer hydrogenation in $CDCl_3$ as apolar organic solvent was explored first with quinoline **10** and Hantzsch ester **16** (Figure 1, Table 2, entries 1–8, Supporting Information Figure S13 and Scheme S8). Catalysts were characterized with rate enhancements $re_c = k_{cat}/k_{uncat}$ (Supporting Information Figures S10–S12). With re_c = 1, the original stibine **1a** was inactive under these conditions (Table 2, entry 1). Consistent with deepened σ-holes and increased anion binding, catalysis with stibine **1b** was detectable as re_c = 13.

Moving from stibines to stiboranes, the catalysis of transfer hydrogenation of quinoline **10** in $CDCl_3$ increased to consistent re_c > 100 (Table 2, entries 2–7). Stiboranes outperforming stibines in organic solvents was as expected due to the stronger pnictogen bonds (Table 1, Figure 2), in contrast to trends in membranes and micelles (vide infra).

With substrate **10** in $CDCl_3$, 3,4,5-trifluorophenyl stiboranes **a** were more active than 3,5-bis(trifluoromethyl) phenyls **b**, at least when compared directly with **2** (Table 2, entries 2–7). The counterintuitive finding of equal or even better catalysis with weaker σ acidity, suggested that the misplaced phenyl in substrate **10**, pointing into the concave surface around the σ-hole, was less tolerated on the more crowded surface of the series **b** (Figures 1c and 2e,f). In contrast, **a** < **b** with stibines was consistent with unproblematic accommodation of this bulky substrate on their convex rather than concave surface (Table 2, entry 1, Figures 1a and 2d).

DOI: 10.31635/ccschem.024.202404847
Citation: *CCS Chem.* **2025**, 7, 91–104
Link to VoR: https://doi.org/10.31635/ccschem.024.202404847

Table 3 | *Transport in Lipid Bilayer Membranes*[a]

	T[b]	EC_{50} (μM)[c]	T[b]	EC_{50} (μM)[c]
1	**1a**	0.05 ± 0.01	**1b**	0.6 ± 0.3
2	**2a**	4.3 ± 0.1	**2b**	1.3 ± 0.2
3	**3a**	1.9 ± 0.1	**3b**	0.3 ± 0.1
4	—	—	**4b**	0.2 ± 0.1
5	**5a**	0.15 ± 0.05	—	—
6	—	—	**6b**	0.4 ± 0.1
7	**7a**	0.03 ± 0.01	—	—
8	—	—	**8b**	0.02 ± 0.003

[a] Measured by fluorescence kinetics using the HPTS assay in EYPC-LUVs. Experimental data: Supporting Information Figures S3–S7 and Table S1.
[b] Transporters.
[c] Effective concentrations, in μM.

For substrate **11** without misplaced phenyls, overall higher catalytic activities were found for both the Sb(III) and the Sb(V) catalysts in $CDCl_3$ (Figure 1, Table 2, entries 1–7, Supporting Information Scheme S9). Significant superiority of stiboranes over stibines in organic solvents was maintained, in agreement with pnictogen bonding (Table 1). With stibines, **1b** remained faster than **1a** (Table 2, entry 1). This was consistent with the assignment of pnictogen bonds as primary and AEDA interactions on the convex surface as secondary interactions for transition-state stabilization (Figures 1a and 2d). With stiboranes in $CDCl_3$, **2a** failed to outperform **2b** as clearly as with **10** (Table 1, entry 2). This was as expected for reduced steric repulsion between the more concave environment and a less misshaped substrate **11** (Figures 1c and 2e,f).

To possibly strengthen pnictogen bonds by dipole–dipole interactions with the solvent, $CDCl_3$ was replaced by the polar aprotic CD_3CN (Table 2, entries 9–11). With substrate **10**, the catalytic activity increased more than one order of magnitude, reaching an absolute maximum at re_c = 9600 for **2a** (Table 2, entry 9). With substrate **10** in CD_3CN, **2a** was still more active than **3a** (Table 2, entry 9 vs 10). This final mismatch with pnictogen bonding was overcome with the less bulky substrate **11** in CD_3CN, which was best converted by **3b**, followed by **3a** > **4b** > **2a** (Table 2, entries 9–11). The order of the latter catalytic performance almost perfectly aligned with the respective σ-holes and global and local polarizability, with **3b** being the best among all of these computed parameters (Table 1, entry 6).

Bismuth, finally, on the Bi(III) level, the σ-acidic bismuthine **8b** was less active than the homologous stibines (Table 2, entry 8). These poor results with σ-acidic bismuthine catalysts were consistent with previous results[32,53] but in conflict with the pnictogen bonding predictions (Table 1, entries 15, 16), anion binding[44] and anion transport (Table 3, entry 9).

Ion transport in lipid bilayer membranes

The liquid-disordered (L_d) EYPC-LUVs were selected for studies in lipid bilayers. Ion transport across EYPC bilayer membranes[1,30,31,46,54–68] was measured using the HPTS assay (Supporting Information Figures S3–S7). This classical fluorescence assay reports on the velocity of the decay of a pH gradient caused by the accelerated transport of anions or cations. For the previously confirmed anion transport by pnictogen bonds in a buffer with NaCl, this meant transmembrane transport of OH^- is compensated by chloride antiport in the other direction. The concentration dependence of the observed activity revealed the EC_{50}, which is the effective transporter concentration needed to reach 50% activity (Table 3).

Ion transport with pnictogen bonds and other σ-hole interactions has been demonstrated by several groups.[30,31,46,64,65,69,70] σ-acidic stibines like **1a** were confirmed to be excellent ion transporters also under the present, unoptimized conditions (Table 3, entry 1). The high transport activity of the σ-acidic bismuthine **8b** (Table 3, entry 8) was intriguing because it was consistent with pnictogen-bonding strength (Table 1) and anion binding,[44] but contrary to the present and previous[12,26,32,43] results on catalysis in organic solvents (Table 2).

Moving from stibines to more σ-acidic stiboranes, ion transport activity failed to increase significantly (Table 3, entries 1 vs 2–7). Also, within the stiborane series, transport activities decreased with increasing depth of the σ-holes (Table 3, entries 2–8) to end up with a very low EC_{50} = 30 ± 10 nM for amide **7a** (Table 3, entry 7) with low V_{max} = +43.2 kcal mol^{-1} (Table 1, entry 13). Weaker ion transport with stronger ion binding has been observed occasionally and treated theoretically earlier on by Lehn and coworkers (vide infra).[71]

While this study was ongoing, Murphy and Gabbaï[46] reported anion transport of the substituent-free triphenyl version of **2**. They showed that one or two methyl groups in the *ortho* position lowered the anion transport. This result was interpreted as support for operational pnictogen bonds.[46] Although measurements under different conditions were not directly comparable, the relatively high activity reported for stiboranes with shallower σ-holes compared with the series used in this study was in agreement with the general trend that ion transport decreased with increased ion binding, that is, the activity in the Goldilocks inverted region (vide infra).

Catalysis in lipid bilayer membranes and micelles

The combination of transport and catalysis is an intriguing topic in supramolecular systems chemistry.[30,60,72–75] Catalysis with stibines in lipid bilayer membranes has been shown previously to be as significant as ion transport, and much more efficient than catalysis in organic solvents.[30] This result was of interest because increases in

DOI: 10.31635/ccschem.024.202404847
Citation: *CCS Chem.* **2025**, 7, 91–104
Link to VoR: https://doi.org/10.31635/ccschem.024.202404847

Table 4 | *Catalysis in Lipid Bilayer Membranes and Micelles*[a]

	S[b]	H[c]	C[d]	m[e]	re_c[f]	re_m[g]	re_{mc}[h]
1	**12**	**17**	**2b**	L_d/Cl^-	12	1.1	12
2	**13**	**17**	**2b**	L_d/Cl^-	380	1.0	380
3	**14**	**17**	**2b**	L_d/Cl^-	130	0.9	130
4	**12**	**17**	**2b**	L_d/SO_4^{2-}	7	1.0	6
5	**13**	**17**	**2b**	L_d/SO_4^{2-}	470	0.9	420
6	**14**	**17**	**2b**	L_d/SO_4^{2-}	150	1.1	110
7	**14**	**16**	**2b**	L_d/SO_4^{2-}	10	0.9	7
8	**15**	**16**	**2b**	L_d/SO_4^{2-}	22	0.8	8
9	**15**	**16**	**2b**	TX/SO_4^{2-}	90	4.8	40
10	**15**	**16**	**3b**	TX/SO_4^{2-}	80	4.8	29
11	**15**	**16**	**4b**	TX/SO_4^{2-}	90	4.8	30
12	**15**	**16**	**1a**	TX/SO_4^{2-}	3.3	4.8	30

[a] Rate enhancements with catalyst (C, re_c), with membranes/micelles (m, re_m), or both (re_{mc}), compared with k_{uncat} in buffer from initial rates determined by fluorescence kinetics in (entries 1–8) EYPC-LUVs (50 μM EYPC), 30 mol % C, HEPES pH 7.0/DMSO 97:3, 40 °C and (entries 1–6) 0.63 mM S, 600 mol % H or (entries 7–8) 0.32 mM S, 300 mol % H, and (entries 9–12) 10% micelles (HEPES pH 7.0/DMSO/Triton X-100 (TX) 8:1:1), 30 mol % C, 30 °C, 1.0 mM S and 300 mol % H. Experimental data: Supporting Information Figures S17–S23.
[b] Quinoline substrates.
[c] Hydride donors.
[d] Catalysts.
[e] Membranes/micelles (L_d: EYPC-LUVs, with 100 mM NaCl or 67 mM Na_2SO_4 in buffer), micelles (Triton X-100, 67 mM Na_2SO_4 in buffer).
[f] $re_c = k_{cat}/k_{uncat}$ for catalyst.
[g] $re_m = k_{cat}/k_{uncat}$ for membranes/micelles as catalyst.
[h] $re_{mc} = k_{cat}/k_{uncat}$ for membranes/micelles and catalyst against buffer.

effective concentration could account only for about half of the rate enhancements observed. Thus, the other half should originate for emergent properties in lipid bilayer membranes, offering desolvated substrates and catalysts for enhanced interactions in a confined, directional, and compartmentalized environment.

Catalysis with stiboranes in lipid bilayer membranes was explored with the same reaction used for characterization in organic solvents, that is, transfer hydrogenation of quinolines (Figure 1f, Table 4). Studies were initiated with the fluorogenic substrate **12**, recently introduced together with the more hydrophilic Hantzsch ester **17** to explore supramolecular system catalysis in water (Supporting Information Scheme S7 and Figures S13–S21).[28] As expected with the solvent competing for pnictogen bonds, the rate enhancements re_c = 12 obtained with stiborane **2b** in water containing neither micelles nor membranes were less important than rate enhancements in organic solvents (Table 4, entry 1 vs Table 2, entry 2). In the presence of EYPC-LUVs but without stiborane **2b**, rate enhancements re_m = 1.1 were negligible (Table 4, entry 1). Rate enhancement re_{mc} = 12 in the presence of stiborane **2b** and EYPC-LUVs did not differ much from the re_c = 12 without vesicles (Table 4, entry 1).

The less hydrophilic substrates **13** and **14** were tested next (Table 4, entries 2, 3, Supporting Information Scheme S6). Their transfer hydrogenation in water was detectable by fluorescence spectroscopy because the reduced products **13p** and **14p** are push–pull fluorophores with redshifted excitation and emission (Figure 1).[29] The rate enhancements were up to re_c = 380 for stiborane **2b** in water and more than one order of magnitude higher compared with **12** (Table 4, entries 1, 2). Addition of membranes did not affect the rate enhancements (Table 4, entries 2, 3).

Replacement of excess chloride in the buffer by sulfate reduced catalysis with **12** and increased catalysis re_c with more hydrophobic **13** and **14** (Table 4, entries 4–6). More importantly, in the presence of sulfates, the catalytic activity re_{mc} of stiborane **2b** in membranes decreased substantially compared with re_c (Table 4, entries 4–6). Compared with re_c, re_{mc} further decreased with more hydrophobic hydride donor **16** (Table 4, entry 7) and quinoline substrate **15** (Table 4, entry 8). These seemingly counterintuitive trends with hydrophobic substrates performing poorly in membranes were mirrored in Triton X-100 micelles for stiborane catalysts **2b**, **3b**, and **4b** (Table 4, entries 9–11).

The Goldilocks principle: entering the inverted region

The failure of σ-acidic stiboranes to transport and transform in membranes and micelles beyond the ordinary

DOI: 10.31635/ccschem.024.202404847
Citation: *CCS Chem.* **2025**, 7, 91–104
Link to VoR: https://doi.org/10.31635/ccschem.024.202404847

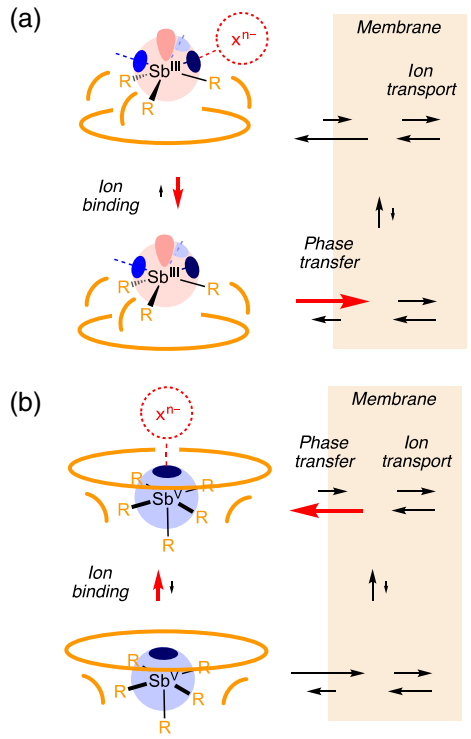

Figure 3 | *Pnictogen-bonding phase transfer primarily accounts for activity in membranes and micelles. (a) σ-Acidic stibines have high activity in membranes despite moderate pnictogen bonding because they enable anion release for favorable phase transfer. (b) σ-Acidic stiboranes have moderate activity in membranes despite strong pnictogen bonding because excessive anion binding inhibits phase transfer into membranes.*

was in sharp contrast to present and previous[30,31] results with σ-acidic stibines (Tables 3 and 4). Also, it was inconsistent with the excellent performance of σ-acidic stiboranes in organic solvents, clearly exceeding that of stibines (Table 2). These opposing results were understandable as a special expression of the Goldilocks principle that originates from phase transfer by excessive pnictogen bonding (Figure 3). Namely, σ-acidic stibines bound anions and anionic transition states not too strongly because they had shallower σ-holes that form weaker pnictogen bonds (Table 1), as testified by less impressive catalysis in organic solvents (Table 2). Thus, in biphasic systems, anion complexes would easily dissociate and release the intrinsically hydrophobic stibines into the hydrophobic phase of membranes or micelles. This favorable phase transfer or partitioning without interference from weak pnictogen bonds boosted effective concentrations as the primary origin of efficient transport and catalysis in membranes (Figure 3a and Tables 3 and 4).

On the contrary, σ-acidic stiboranes possessed deep σ-holes, affording strong pnictogen bonds (Table 1). The resultant strong binding of anions and anionic transition states accounted for excellent catalysis in organic solvents (Table 2). In biphasic systems, these stable stiborane-anion complexes did not dissociate. Their anionic nature provided the hydrophilicity needed for the pnictogen-bonding phase transfer of the intrinsically hydrophobic stiboranes into the aqueous phase (Figure 3b). This pnictogen-bonding phase transfer increased with increasing anion binding, resulting in decreasing activity in membranes with excessive pnictogen bonding (Tables 3 and 4).

The inactivation of stiboranes but not stibines by direct competitive binding to lipids and detergents as a possible alternative explanation was not convincing. Charge-neutral rather than anionic lipids and detergents were used to minimize possible competition for pnictogen bonding to anions and anionic transition states down to the level of water binding. In water, however, including 67 mM sulfate, stibine catalysts remained as inferior to stiboranes as in apolar solvents (Table 4, re_c, entry 12 vs 8–11). Only in micelles and membrane, stibine catalysts accelerated and stiboranes slowed down (Table 4, re_{mc} vs re_c, entry 12 vs 8–11). These opposing trends in the water against micelles and membranes were not explained by direct competitive pnictogen bonding into the environment, solvents, and beyond. Thus, these findings supported pnictogen-bonding phase transfer as the origin of the observed Goldilocks behavior in biphasic systems (Figure 3). Increasing catalysis from stibines to stiboranes in a homogenous solution further illustrated that the Goldilocks principle for function in biphasic systems was, although obviously related, not the same as the principle of Sabatier,[76–78] or general homogenous anticatalysis concepts based on ground-state stabilization exceeding transition-state stabilization.[79]

The dependence of ion transport on ion binding in membranes has been assessed theoretically by Lehn and coworkers.[71] Their Goldilocks principle[60,69] predicted that for weak ion binding in the normal region, transport improves with binding, while for strong binding in the inverted region, transport deteriorates with increasing binding (Figure 4). While activity in the normal region

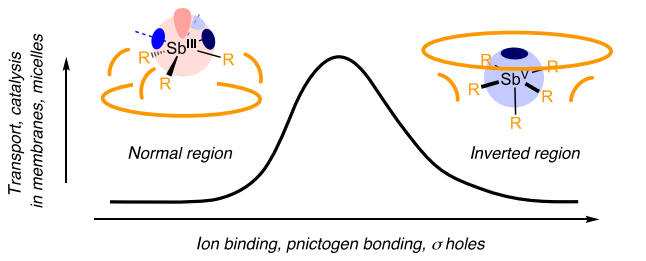

Figure 4 | *The Goldilocks principle for activity in membranes and micelles, with σ-acidic stibines operating in the normal and stiboranes in the inverted region.*

DOI: 10.31635/ccschem.024.202404847
Citation: *CCS Chem.* **2025**, 7, 91–104
Link to VoR: https://doi.org/10.31635/ccschem.024.202404847

has been described in many variations,[80,81] the Goldilocks inverted region has attracted less attention.[57,60,69,80,82] Our present results provide complete and coherent experimental coverage of the Goldilocks principle: Whereas stibines operate in the normal region, the more σ-acidic stiboranes enter deep into the Goldilocks inverted region.

This unlocking of the Goldilocks inverted region explained all results reported in this study with quite remarkable consistency. Transport activity decreased with increasing pnictogen bonding from Sb(III) to Sb(V), as well as within the stiborane series (Table 3). The Goldilocks principle was also compatible with catalysis in membranes and micelles. Particularly impressive was the decrease in activity of Sb(V) catalysts in membranes upon changing from chloride to sulfate in the aqueous phase (Table 4, entries 1–6). Higher stability and charge of stiborane-sulfate compared with stiborane-chloride complexes shifted equilibria and increased hydrophilicity to maximize pnictogen-bonding phase transfer into water (Figure 3b). Catalysis with more hydrophobic substrates was less efficient in the presence of membranes because they were better separated from the stiborane-anion complexes in the aqueous phase (Table 4, entries 7, 8). As another example, the similarly poor performance of σ-acidic stiboranes in micelles and membranes supported that the Goldilocks principle applied, independent of suprastructural differences of the two apolar phases.

The Goldilocks principle would then imply that contrary to stiborane catalysts in the inverted region, catalysis with σ-acidic stibines in the normal region should improve not only in membranes[30] but also in micelles. This last open question within the covered functional space was addressed by transfer hydrogenation of quinoline **15** with donor **16** and catalyst **1a**. The re_c = 3.3 without micelles increased almost 10 times to the re_{mc} = 30 in the presence of Triton X-100 micelles (Table 4, entry 12, Supporting Information Figures S22 and S23). This control in the Goldilocks normal region was important because it provided corroborative evidence for the generality and robustness of the Goldilocks principle, confirming compatibility with catalysis as general, independent of the reactions, and in normal and inverted regions in micelles.

Conclusions

The objective of this study was to compare the activities of pnictogen-bonding Sb(III) and Sb(V) catalysts and transporters in organic solvents and lipid bilayer membranes. The main missing data was comparative ion transport and catalysis of σ-acidic stiboranes in membranes. Their catalytic activity in organic solvents was shown to exceed that of σ-acidic stibines, as expected from their stronger pnictogen bonds. For ion transport in membrane, σ-acidic stibines outperformed σ-acidic stiboranes, and transport within the stiborane series decreased with increasing pnictogen bonding. While catalysis by stibines increased in membranes and micelles, catalysis by stiboranes generally decreased. Overall, decreasing activity in membranes with increasingly strong pnictogen bonds was explained with pnictogen-bonding phase transfer. Excessive pnictogen-bonding yielded stable hydrophilic pnictogen-bonded stiborane-anion complexes that extracted the hydrophobic stiboranes from the membrane into the aqueous phase. This behavior placed σ-acidic stiboranes in the inverted region of the Goldilocks principle, characterized by decreasing activity with increasing binding. While σ-acidic stibines operated in the not further remarkable Goldilocks normal region, general access to the Goldilocks inverted region with σ-acidic stiboranes, covering not only transport but also catalysis in not only membranes but also micelles, was unprecedented. The importance of the found general validity of the Goldilocks principle for activity in biphasic systems to design and interpret supramolecular function cannot be overestimated.

The comprehensive exploration of the Goldilocks inverted region for function in biphasic systems further confirmed the obvious: More is not always better, stronger pnictogen bonds do not have to equal better performance. From this point of view, entering the Goldilocks inverted region when approaching the transition from noncovalent pnictogen bonding interactions to covalent ligand binding could be seen as a wonderful testimony of the power of supramolecular chemistry to access new functions.

Supporting Information

Supporting Information is available and includes synthesis, characterization, crystallography, computational modeling, reaction kinetics procedures [NMR, ultraviolet (UV), fluorescence spectroscopy], and ion transport in bilayer membranes (HPTS assay). Supplementary crystallographic data for deposition were submitted to the Cambridge Crystallographic Data Centre [(CCDC); **2a**: CCDC 2370744, **3a**: CCDC 2370743, **3b**: CCDC 2370742] and supplementary crystallographic data for this paper are attached as PDF format of the crystallographic information file (CIF), which include **2a**, **3a**, and **3b**.

Conflict of Interest

There is no conflict of interest to report.

DOI: 10.31635/ccschem.024.202404847
Citation: *CCS Chem.* **2025**, 7, 91–104
Link to VoR: https://doi.org/10.31635/ccschem.024.202404847

Funding Information

This research was supported by the University of Geneva, the National Centre of Competence in Research (NCCR) Molecular Systems Engineering, Switzerland (grant no. 51NF40-205608), the Swiss National Science Foundation (NSF; Swiss-ERC Advanced Grant TIMEUP, TMAG-2_209190; Excellence Grant 200020 204175), and the Spain Ministry of Science, Innovation and Universities (MICIU/AEI of Spain; project PID2020-115637GB-I00 FEDER funds).

Acknowledgments

We thank the NMR, mass spectrometry (MS), and X-ray platforms for their services, and the University of Geneva, Switzerland, the NCCR Molecular Systems Engineering, the Swiss NSF, and the MICIU/AEI of Spain for financial support.

References

1. Murphy, B. L.; Gabbaï, F. P. Binding, Sensing, and Transporting Anions with Pnictogen Bonds: The Case of Organoantimony Lewis Acids. *J. Am. Chem. Soc.* **2023**, *145*, 19458–19477.
2. Jovanovic, D.; Mohanan, M. P.; Huber, S. M. Halogen, Chalcogen, Pnictogen, and Tetrel Bonding in Non-Covalent Organocatalysis: An Update. *Angew. Chem. Int. Ed.* **2024**, *63*, e202404823.
3. Breugst, M.; Koenig, J. J. σ-Hole Interactions in Catalysis. *Eur. J. Org. Chem.* **2020**, *2020*, 5473–5487.
4. Taylor, M. S. Anion Recognition Based on Halogen, Chalcogen, Pnictogen and Tetrel Bonding. *Coord. Chem. Rev.* **2020**, *413*, 213270.
5. Lim, J. Y. C.; Beer, P. D. Sigma-Hole Interactions in Anion Recognition. *Chem* **2018**, *4*, 731–783.
6. Bauzá, A.; Mooibroek, T. J.; Frontera, A. The Bright Future of Unconventional σ/π-Hole Interactions. *ChemPhysChem* **2015**, *16*, 2496–2517.
7. Cavallo, G.; Metrangolo, P.; Milani, R.; Pilati, T.; Priimagi, A.; Resnati, G.; Terraneo, G. The Halogen Bond. *Chem. Rev.* **2016**, *116*, 2478–2601.
8. Bamberger, J.; Ostler, F.; García Mancheño, O. Frontiers in Halogen and Chalcogen-Bond Donor Organocatalysis. *ChemCatChem* **2019**, *11*, 5198–5211.
9. Biot, N.; Bonifazi, D. Chalcogen-Bond Driven Molecular Recognition at Work. *Coord. Chem. Rev.* **2020**, *413*, 213243.
10. Liu, C.-Z.; Koppireddi, S.; Wang, H.; Zhang, D.-W.; Li, Z.-T. Halogen Bonding Directed Supramolecular Quadruple and Double Helices from Hydrogen-Bonded Arylamide Foldamers. *Angew. Chem. Int. Ed.* **2019**, *58*, 226–230.
11. Benz, S.; Poblador-Bahamonde, A. I.; Low-Ders, N.; Matile, S. Catalysis with Pnictogen, Chalcogen, and Halogen Bonds. *Angew. Chem. Int. Ed.* **2018**, *57*, 5408–5412.
12. Yang, M.; Tofan, D.; Chen, C.-H.; Jack, K. M.; Gabbaï, F. P. Digging the Sigma-Hole of Organoantimony Lewis Acids by Oxidation. *Angew. Chem. Int. Ed.* **2018**, *57*, 13868–13872.
13. Zhang, J.; Wei, J.; Ding, W.-Y.; Li, S.; Xiang, S.-H.; Tan, B. Asymmetric Pnictogen-Bonding Catalysis: Transfer Hydrogenation by a Chiral Antimony(V) Cation/Anion Pair. *J. Am. Chem. Soc.* **2021**, *143*, 6382–6387.
14. Zhang, Y.; Zhu, H.; Zhang, B.; Yang, H.; Tan, C.-H.; Wang, C.; Wen, J.; Zong, L. Hydrogen Bond-Enhanced Halogen Bonding Organocatalyst with C(Sp^3)–Br and Sulfoxide Moieties. *ACS Catal.* **2023**, *13*, 7103–7109.
15. Pale, P.; Mamane, V. Chalcogen Bonding Catalysis: Tellurium, the Last Frontier? *Chem. – Eur. J.* **2023**, *29*, e202302755.
16. Sutar, R. L.; Huber, S. M. Catalysis of Organic Reactions Through Halogen Bonding. *ACS Catal.* **2019**, *9*, 9622–9639.
17. Keuper, A. C.; Fengler, K.; Ostler, F.; Danelzik, T.; Piekarski, D. G.; García Mancheño, O. Fine-Tuning Substrate–Catalyst Halogen–Halogen Interactions for Boosting Enantioselectivity in Halogen-Bonding Catalysis. *Angew. Chem. Int. Ed.* **2023**, *62*, e202304781.
18. Bruckmann, A.; Pena, M. A.; Bolm, C. Organocatalysis Through Halogen-Bond Activation. *Synlett* **2008**, *19*, 900–902.
19. Weiss, R.; Aubert, E.; Pale, P.; Mamane, V. Chalcogen-Bonding Catalysis with Telluronium Cations. *Angew. Chem. Int. Ed.* **2021**, *60*, 19281–19286.
20. He, W.; Ge, Y.-C.; Tan, C.-H. Halogen-Bonding-Induced Hydrogen Transfer to C═N Bond with Hantzsch Ester. *Org. Lett.* **2014**, *16*, 3244–3247.
21. Kerckhoffs, A.; Moss, I.; Langton, M. J. Photo-Switchable Anion Binding and Catalysis with a Visible Light Responsive Halogen Bonding Receptor. *Chem. Commun.* **2022**, *59*, 51–54.
22. Liu, J.; Deng, R.; Liang, X.; Zhou, M.; Zheng, P.; Chi, Y. R. Carbene-Catalyzed and Pnictogen Bond-Assisted Access to P^{III}-Stereogenic Compounds. *Angew. Chem. Int. Ed.* **2024**, *63*, e202404477.
23. Guo, H.; Kirchhoff, J.-L.; Strohmann, C.; Grabe, B.; Loh, C. C. J. Exploiting π and Chalcogen Interactions for the β-Selective Glycosylation of Indoles Through Glycal Conformational Distortion. *Angew. Chem. Int. Ed.* **2024**, *63*, e202316667.
24. Zhao, Z.; Wang, Y. Chalcogen Bonding Catalysis with Phosphonium Chalcogenide (PCH). *Acc. Chem. Res.* **2023**, *56*, 608–621.
25. Tu, Y.-L.; Zhang, B.-B.; Qiu, B.-S.; Wang, Z.-X.; Chen, X.-Y. Cross-Electrophile C–P(III) Coupling of Chlorophosphines with Organic Halides: Photoinduced P(III) and Aminoalkyl Radical Generation Enabled by Pnictogen Bonding. *Angew. Chem. Int. Ed.* **2023**, *62*, e202310764.
26. Chen, H.; Frontera, A.; Gutiérrez López, M. Á.; Sakai, N.; Matile, S. Pnictogen-Bonding Catalysts, Compared to Tetrel-Bonding Catalysts: More Than Just Weak Lewis Acids. *Helv. Chim. Acta* **2022**, *105*, e202200119.
27. Bergamaschi, G.; Lascialfari, L.; Pizzi, A.; Espinoza, M. I. M.; Demitri, N.; Milani, A.; Gori, A.; Metrangolo, P. A Halogen Bond-Donor Amino Acid for Organocatalysis in Water. *Chem. Commun.* **2018**, *54*, 10718–10721.

DOI: 10.31635/ccschem.024.202404847
Citation: *CCS Chem.* **2025**, 7, 91–104
Link to VoR: https://doi.org/10.31635/ccschem.024.202404847

28. Renno, G.; Zhang, Q.-X.; Frontera, A.; Sakai, N.; Matile, S. A Fluorogenic Substrate for Quinoline Reduction: Pnictogen-Bonding Catalysis in Aqueous Systems. *Helv. Chim. Acta* **2024**, *107*, e202400015.
29. Renno, G.; Chen, D.; Zhang, Q.-X.; Gomila, R. M.; Frontera, A.; Sakai, N.; Ward, T. R.; Matile, S. Pnictogen-Bonding Enzymes. *Angew. Chem. Int. Ed.* **2024**, *63*, e202411347.
30. Humeniuk, H. V.; Gini, A.; Hao, X.; Coelho, F.; Sakai, N.; Matile, S. Pnictogen-Bonding Catalysis and Transport Combined: Polyether Transporters Made in Situ. *JACS Au* **2021**, *1*, 1588–1593.
31. Lee, L. M.; Tsemperouli, M.; Poblador-Bahamonde, A. I.; Benz, S.; Sakai, N.; Sugihara, K.; Matile, S. Anion Transport with Pnictogen Bonds in Direct Comparison with Chalcogen and Halogen Bonds. *J. Am. Chem. Soc.* **2019**, *141*, 810–814.
32. Gini, A.; Paraja, M.; Galmés, B.; Besnard, C.; Poblador-Bahamonde, A. I.; Sakai, N.; Frontera, A.; Matile, S. Pnictogen-Bonding Catalysis: Brevetoxin-Type Polyether Cyclizations. *Chem. Sci.* **2020**, *11*, 7086–7091.
33. Lascano, S.; Zhang, K.-D.; Wehlauch, R.; Gademann, K.; Sakai, N.; Matile, S. The Third Orthogonal Dynamic Covalent Bond. *Chem. Sci.* **2016**, *7*, 4720–4724.
34. Trowbridge, A.; Reich, D.; Gaunt, M. J. Multicomponent Synthesis of Tertiary Alkylamines by Photocatalytic Olefin-Hydroaminoalkylation. *Nature* **2018**, *561*, 522–527.
35. Perdew, J. P. Density-Functional Approximation for the Correlation Energy of the Inhomogeneous Electron Gas. *Phys. Rev. B* **1986**, *33*, 8822–8824.
36. Becke, A. D. Density-Functional Thermochemistry. IV. A New Dynamical Correlation Functional and Implications for Exact-Exchange Mixing. *J. Chem. Phys.* **1996**, *104*, 1040–1046.
37. Ahlrichs, R.; Bär, M.; Häser, M.; Horn, H.; Kölmel, C. Electronic Structure Calculations on Workstation Computers: The Program System Turbomole. *Chem. Phys. Lett.* **1989**, *162*, 165–169.
38. Grimme, S.; Antony, J.; Ehrlich, S.; Krieg, H. A Consistent and Accurate Ab Initio Parametrization of Density Functional Dispersion Correction (DFT-D) for the 94 Elements H-Pu. *J. Chem. Phys.* **2010**, *132*, 154104.
39. Frisch, M. J.; Trucks, G. W.; Schlegel, H. B.; Scuseria, G. E.; Robb, M. A.; Cheeseman, J. R.; Scalmani, G.; Barone, V.; Petersson, G. A.; Nakatsuji, H.; Li, X.; Caricato, M.; Marenich, A. V.; Bloino, J.; Janesko, B. G.; Gomperts, R.; Mennucci, B.; Hratchian, H. P.; Ortiz, J. V.; Izmaylov, A. F.; Sonnenberg, J. L.; Williams; Ding, F.; Lipparini, F.; Egidi, F.; Goings, J.; Peng, B.; Petrone, A.; Henderson, T.; Ranasinghe, D.; Zakrzewski, V. G.; Gao, J.; Rega, N.; Zheng, G.; Liang, W.; Hada, M.; Ehara, M.; Toyota, K.; Fukuda, R.; Hasegawa, J.; Ishida, M.; Nakajima, T.; Honda, Y.; Kitao, O.; Nakai, H.; Vreven, T.; Throssell, K.; Montgomery, J. A. Jr.; Peralta, J. E.; Ogliaro, F.; Bearpark, M. J.; Heyd, J. J.; Brothers, E. N.; Kudin, K. N.; Staroverov, V. N.; Keith, T. A.; Kobayashi, R.; Normand, J.; Raghavachari, K.; Rendell, A. P.; Burant, J. C.; Iyengar, S. S.; Tomasi, J.; Cossi, M.; Millam, J. M.; Klene, M.; Adamo, C.; Cammi, R.; Ochterski, J. W.; Martin, R. L.; Morokuma, K.; Farkas, O.; Foresman, J. B.; Fox, D. J. *Gaussian 16 Rev. C.01*; Gaussian, Inc.: Wallingford, CT, **2016**.
40. Adamo, C.; Barone, V. Toward Reliable Density Functional Methods Without Adjustable Parameters: The PBE0 Model. *J. Chem. Phys.* **1999**, *110*, 6158–6170.
41. Lu, T.; Chen, F. Multiwfn: A Multifunctional Wavefunction Analyzer. *J. Comput. Chem.* **2012**, *33*, 580–592.
42. Benz, S.; López-Andarias, J.; Mareda, J.; Sakai, N.; Matile, S. Catalysis with Chalcogen Bonds. *Angew. Chem. Int. Ed.* **2017**, *56*, 812–815.
43. Chen, H.; Li, T.-R.; Sakai, N.; Besnard, C.; Guénée, L.; Pupier, M.; Viger-Gravel, J.; Tiefenbacher, K.; Matile, S. Decoded Fingerprints of Hyperresponsive, Expanding Product Space: Polyether Cascade Cyclizations as Tools to Elucidate Supramolecular Catalysis. *Chem. Sci.* **2022**, *13*, 10273–10280.
44. Kuhn, H.; Docker, A.; Beer, P. D. Anion Recognition with Antimony(III) and Bismuth(III) Triaryl-Based Pnictogen Bonding Receptors. *Chem. – Eur. J.* **2022**, *28*, e202201838.
45. Gademann, K. Copy, Edit, and Paste: Natural Product Approaches to Biomaterials and Neuroengineering. *Acc. Chem. Res.* **2015**, *48*, 731–739.
46. Murphy, B. L.; Gabbaï, F. P. Tunable Pnictogen Bonding at the Service of Hydroxide Transport Across Phospholipid Bilayers. *J. Am. Chem. Soc.* **2024**, *146*, 7146–7151.
47. Cordero, B.; Gómez, V.; Platero-Prats, A. E.; Revés, M.; Echeverría, J.; Cremades, E.; Barragán, F.; Alvarez, S. Covalent Radii Revisited. *Dalton Trans.* **2008**, *37*, 2832–2838.
48. Gabriel, G. J.; Iverson, B. L. Aromatic Oligomers That Form Hetero Duplexes in Aqueous Solution. *J. Am. Chem. Soc.* **2002**, *124*, 15174–15175.
49. Hagihara, S.; Tanaka, H.; Matile, S. Boronic Acid Converters for Reactive Hydrazide Amplifiers: Polyphenol Sensing in Green Tea with Synthetic Pores. *J. Am. Chem. Soc.* **2008**, *130*, 5656–5657.
50. Wang, D.-X.; Wang, M.-X. Exploring Anion–π Interactions and Their Applications in Supramolecular Chemistry. *Acc. Chem. Res.* **2020**, *53*, 1364–1380.
51. Tuo, D.-H.; Tang, S.; Jin, P.; Li, J.; Wang, X.; Zhang, C.; Ao, Y.-F.; Wang, Q.-Q.; Wang, D.-X. π-Pimer, π-Dimer, π-Trimer, and 1D π-Stacks in a Series of Benzene Triimide Radical Anions: Substituent-Modulated π Interactions and Physical Properties in Crystalline State. *CCS Chem.* **2022**, *5*, 1343–1352.
52. Tan, M.-L.; Gutiérrez López, M. Á.; Sakai, N.; Matile, S. Anion-(π)n-π Catalytic Micelles. *Angew. Chem. Int. Ed.* **2023**, *62*, e202310393.
53. Sharma, D.; Balasubramaniam, S.; Kumar, S.; Jemmis, E. D.; Venugopal, A. Reversing Lewis Acidity from Bismuth to Antimony. *Chem. Commun.* **2021**, *57*, 8889–8892.
54. Docker, A.; Langton, M. J. Transmembrane Anion Transport Mediated by Sigma-Hole Interactions. *Trends Chem.* **2023**, *5*, 792–794.
55. de Jong, J.; Bos, J. E.; Wezenberg, S. J. Stimulus-Controlled Anion Binding and Transport by Synthetic Receptors. *Chem. Rev.* **2023**, *123*, 8530–8574.
56. Davis, J. T.; Gale, P. A.; Quesada, R. Advances in Anion Transport and Supramolecular Medicinal Chemistry. *Chem. Soc. Rev.* **2020**, *49*, 6056–6086.
57. Valkenier, H.; Judd, L. W.; Li, H.; Hussain, S.; Sheppard, D. N.; Davis, A. P. Preorganized Bis-Thioureas as Powerful

DOI: 10.31635/ccschem.024.202404847
Citation: *CCS Chem.* **2025**, 7, 91–104
Link to VoR: https://doi.org/10.31635/ccschem.024.202404847

Anion Carriers: Chloride Transport by Single Molecules in Large Unilamellar Vesicles. *J. Am. Chem. Soc.* **2014**, *136*, 12507–12512.
58. Wezenberg, S. J.; Chen, L.-J.; Bos, J. E.; Feringa, B. L.; Howe, E. N. W.; Wu, X.; Siegler, M. A.; Gale, P. A. Photomodulation of Transmembrane Transport and Potential by Stiff-Stilbene Based Bis(Thio)Ureas. *J. Am. Chem. Soc.* **2022**, *144*, 331–338.
59. Huang, W.-L.; Wang, X.-D.; Ao, Y.-F.; Wang, Q.-Q.; Wang, D.-X. Artificial Chloride-Selective Channel: Shape and Function Mimic of the ClC Channel Selective Pore. *J. Am. Chem. Soc.* **2020**, *142*, 13273–13277.
60. Chao, X.; Johnson, T. G.; Temian, M.-C.; Docker, A.; Wallabregue, A. L. D.; Scott, A.; Conway, S. J.; Langton, M. J. Coupling Photoresponsive Transmembrane Ion Transport with Transition Metal Catalysis. *J. Am. Chem. Soc.* **2024**, *146*, 4351–4356.
61. Wu, X.; Howe, E. N. W.; Gale, P. A. Supramolecular Transmembrane Anion Transport: New Assays and Insights. *Acc. Chem. Res.* **2018**, *51*, 1870–1879.
62. Sato, K.; Muraoka, T.; Kinbara, K. Supramolecular Transmembrane Ion Channels Formed by Multiblock Amphiphiles. *Acc. Chem. Res.* **2021**, *54*, 3700–3709.
63. Cataldo, A.; Norvaisa, K.; Halgreen, L.; Bodman, S. E.; Bartik, K.; Butler, S. J.; Valkenier, H. Transmembrane Transport of Inorganic Phosphate by a Strapped Calix[4]Pyrrole. *J. Am. Chem. Soc.* **2023**, *145*, 16310–16314.
64. Sharma, R.; Sarkar, S.; Chattopadhayay, S.; Mondal, J.; Talukdar, P. A Halogen-Bond-Driven Artificial Chloride-Selective Channel Constructed from 5-Iodoisophthalamide-Based Molecules. *Angew. Chem. Int. Ed.* **2024**, *63*, e202319919.
65. Ren, C.; Ding, X.; Roy, A.; Shen, J.; Zhou, S.; Chen, F.; Li, S. F. Y.; Ren, H.; Yang, Y. Y.; Zeng, H. A Halogen Bond-Mediated Highly Active Artificial Chloride Channel with High Anticancer Activity. *Chem. Sci.* **2018**, *9*, 4044–4051.
66. Yan, Z.-J.; Li, Y.-W.; Yang, M.; Fu, Y.-H.; Wen, R.; Wang, W.; Li, Z.-T.; Zhang, Y.; Hou, J.-L. Voltage-Driven Flipping of Zwitterionic Artificial Channels in Lipid Bilayers to Rectify Ion Transport. *J. Am. Chem. Soc.* **2021**, *143*, 11332–11336.
67. Peters, A. D.; Borsley, S.; Sala, F. d.; Cairns-Gibson, D. F.; Leonidou, M.; Clayden, J.; Whitehead, G. F. S.; Vitórica-Yrezábal, I. J.; Takano, E.; Burthem, J.; Cockroft, S. L.; Webb, S. J. Switchable Foldamer Ion Channels with Antibacterial Activity. *Chem. Sci.* **2020**, *11*, 7023–7030.
68. Su, D.-D.; Ulrich, S.; Barboiu, M. Bis-Alkylureido Imidazole Artificial Water Channels. *Angew. Chem. Int. Ed.* **2023**, *62*, e202306265.
69. Vargas Jentzsch, A.; Emery, D.; Mareda, J.; Metrangolo, P.; Resnati, G.; Matile, S. Ditopic Ion Transport Systems: Anion–π Interactions and Halogen Bonds at Work. *Angew. Chem. Int. Ed.* **2011**, *50*, 11675–11678.
70. Bickerton, L. E.; Docker, A.; Sterling, A. J.; Kuhn, H.; Duarte, F.; Beer, P. D.; Langton, M. J. Highly Active Halogen Bonding and Chalcogen Bonding Chloride Transporters with Non-Protonophoric Activity. *Chem. Eur. J.* **2021**, *27*, 11738–11745.
71. Behr, J. P.; Kirch, M.; Lehn, J. M. Carrier-Mediated Transport Through Bulk Liquid Membranes: Dependence of Transport Rates and Selectivity on Carrier Properties in a Diffusion-Limited Process. *J. Am. Chem. Soc.* **1985**, *107*, 241–246.
72. Baumeister, B.; Sakai, N.; Matile, S. P-Octiphenyl β-Barrels with Ion Channel and Esterase Activity. *Org. Lett.* **2001**, *3*, 4229–4232.
73. Johnson, T. G.; Sadeghi-Kelishadi, A.; Langton, M. J. Length Dependent Reversible off–on Activation of Photo-Switchable Relay Anion Transporters. *Chem. Commun.* **2024**, *60*, 7160–7163.
74. Litvinchuk, S.; Bollot, G.; Mareda, J.; Som, A.; Ronan, D.; Shah, M. R.; Perrottet, P.; Sakai, N.; Matile, S. Thermodynamic and Kinetic Stability of Synthetic Multifunctional Rigid-Rod β-Barrel Pores: Evidence for Supramolecular Catalysis. *J. Am. Chem. Soc.* **2004**, *126*, 10067–10075.
75. Bravin, C.; Duindam, N.; Hunter, C. A. Artificial Transmembrane Signal Transduction Mediated by Dynamic Covalent Chemistry. *Chem. Sci.* **2021**, *12*, 14059–14064.
76. Sabatier, P. Hydrogénations et Déshydrogénations Par Catalyse. *Berichte Dtsch. Chem. Ges.* **1911**, *44*, 1984–2001.
77. Wodrich, M. D.; Sawatlon, B.; Busch, M.; Corminboeuf, C. The Genesis of Molecular Volcano Plots. *Acc. Chem. Res.* **2021**, *54*, 1107–1117.
78. Murphy, M. A.; Gathmann, S. R.; Getman, R.; Grabow, L.; Abdelrahman, O. A.; Dauenhauer, P. J. Catalytic Resonance Theory: The Catalytic Mechanics of Programmable Ratchets. *Chem. Sci.* **2024**, *15*, 13872–13888.
79. Wolfenden, R.; Snider, M. J. The Depth of Chemical Time and the Power of Enzymes as Catalysts. *Acc. Chem. Res.* **2001**, *34*, 938–945.
80. Li, H.; Valkenier, H.; Thorne, A. G.; Dias, C. M.; Cooper, J. A.; Kieffer, M.; Busschaert, N.; Gale, P. A.; Sheppard, D. N.; Davis, A. P. Anion Carriers as Potential Treatments for Cystic Fibrosis: Transport in Cystic Fibrosis Cells, and Additivity to Channel-Targeting Drugs. *Chem. Sci.* **2019**, *10*, 9663–9672.
81. Míšek, J.; Vargas Jentzsch, A.; Sakurai, S.; Emery, D.; Mareda, J.; Matile, S. A Chiral and Colorful Redox Switch: Enhanced π Acidity in Action. *Angew. Chem. Int. Ed.* **2010**, *49*, 7680–7683.
82. Kirch, M.; Lehn, J.-M. Selective Transport of Alkali Metal Cations through a Liquid Membrane by Macrobicyclic Carriers. *Angew. Chem. Int. Ed.* **1975**, *14*, 555–556.

DOI: 10.31635/ccschem.024.202404847
Citation: *CCS Chem.* **2025**, 7, 91–104
Link to VoR: https://doi.org/10.31635/ccschem.024.202404847